ARTICLE NO. 78-1165R

Comparison of Multiequation Turbulence Models for Several Shock Boundary-Layer Interaction Flows

J.R. Viegas* and C.C. Horstman*
NASA Ames Research Center, Moffett Field, Calif.

Several multiequation eddy viscosity models of turbulence are used with Navier-Stokes equations to compute three classes of experimentally documented shock-separated turbulent boundary-layer flows. The types of flow studied are 1) a normal shock at transonic speeds in both a circular duct and a two-dimensional channel, 2) an incident oblique shock at supersonic speeds on a flat surface, and 3) a two-dimensional compression corner at supersonic speeds. Established zero-equation (algebraic), one-equation (kinetic energy), and two-equation (kinetic energy plus length scale) turbulence models are each utilized to describe the Reynolds shear stress for the three classes of flows. These models are assessed by comparing the calculated values of skin friction, wall pressure distribution, velocity, Mach number, and turbulent kinetic energy profiles with experimental measurements. Of the models tested the two-equation model results gave the best overall agreement with the data.

Introduction

IN recent years, advances in the efficiency of computer solution algorithms[1] for the viscous gasdynamics equations have enabled computing times to be reduced substantially and have thus facilitated systematic studies of turbulence models for complex flowfields. This paper presents such a study comparing numerical solutions of the Reynolds-averaged Navier-Stokes equations with experimental data for several types of flow in which a shock wave interacts with and causes the separation of a turbulent boundary layer. Several turbulence models are used to describe the Reynolds shear stress for these flows. The models are assessed by their ability to predict skin friction, wall-pressure distribution, velocity, Mach number, and turbulent kinetic energy profiles for extensively documented experiments.

The experimental flows studied are illustrated schematically in Figs. 1-4. They are thoroughly documented flows in the sense that both surface and mean-flow quantities were measured; the upstream flow conditions were measured and a fully developed turbulent boundary layer verified ahead of the interaction portion of the flowfield. Fluctuating flowfield measurements were also obtained for two of the experiments. The first experimental flow (shown in Fig. 1), conducted at Ames Research Center, consists of a transonic normal shock-wave boundary-layer interaction (SBLI) in a circular duct at an upstream Mach number of about 1.4.[2] The second (Fig. 2), conducted at California Institute of Technology, is also a transonic normal shock-wave boundary-layer interaction but in a two-dimensional channel at a Mach number of about 1.5 (Ref. 3). The third experiment (Fig. 3), conducted at Princeton University, consists of a supersonic shock-wave boundary-layer interaction flow induced by a two-dimensional compression corner at a Mach number of about 3.[4-6] The fourth experiment (Fig. 4), conducted at Ames Research Center, consists of a supersonic oblique shock-wave boundary-layer interaction in a two-dimensional supersonic channel at a freestream Mach number of about 3.[7-9]

To calculate these flows, sets of zero-, one-, and two-equation eddy viscosity models of turbulence are incorporated into the Reynolds-averaged compressible Navier-Stokes equations which are solved numerically in time until a steady solution is obtained. For the zero-equation models, the eddy viscosity function is related algebraically to the mean-flow variables. The one-equation model use an additional partial differential equation for the kinetic energy of the turbulence to define the velocity scale used in the eddy viscosity formula and the length scale is prescribed algebraically. The two-equation models uses an additional variable and an associated partial differential equation to determine the length scale. Many subclasses of two-equation models can be identified according to how the length scale is defined.

In a recent publication[10] the authors participated in an evaluation of three of these models (the zero-, one-, and Jones-Launder two-equation models) for two of the experimental flows considered in this paper (the axially symmetric transonic flow and the supersonic compression corner flow). Throughout this earlier study there was no apparent superiority of one of these models over the other. Instead, some models seemed superior for specific experimental test cases and inferior for others. It is expected, however, due to their greater versatility, that two-equation models should be applicable to a wider class of complex flows; consequently, other two-equation models are currently under investigation. Of these, the recently developed Wilcox-Rubesin model[11] looks most promising since it was developed to apply to boundary-layer flows influenced by severe adverse pressure gradients as well as to equilibrium flows. The present paper includes results for the two-equation Wilcox-Rubesin model and examines two additional experiments. This is as the first application of the Wilcox-Rubesin two-equation turbulence model to SBLI flows with separation. Included in this paper are comparisons of profiles of velocity, and kinetic energy of turbulence, as well as surface pressure and skin friction for each turbulence model (where applicable) with measurements for each experiment. Finally, an evaluation of the relative usefulness of the various models to predict SBLI flows is presented.

Analysis

Governing Equations

The differential equations used to describe the mean flow for this study are the time-dependent, mass-averaged Navier-Stokes equations for plane or axially symmetric flow of a

Received July 10, 1978; presented as Paper 78-1165 at the AIAA 11th Fluid and Plasma Dynamics Conference, Seattle, Wash., July 10-12, 1978; revision received Feb. 16, 1979.

Index categories: Boundary Layers and Convective Heat Transfer—Turbulent; Computational Methods.

*Research Scientist. Member AIAA.

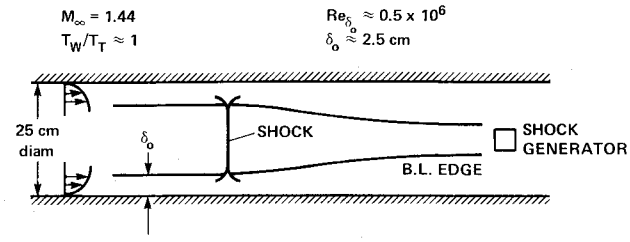

Fig. 1 Sketch of axisymmetric, transonic, normal shock-wave boundary-layer interaction experiment.

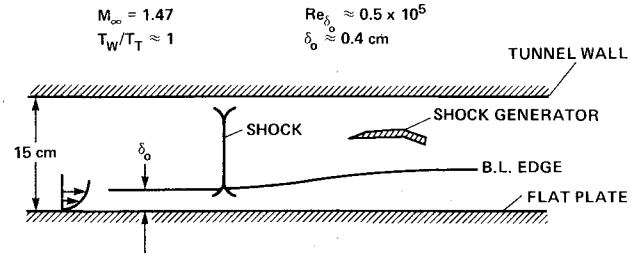

Fig. 2 Sketch of two-dimensional, transonic, normal shock-wave boundary-layer interaction experiment.

compressible fluid. Depending on the turbulence model used, these equations are augumented by additional equations; that is, the one-equation or kinetic-energy model employs one additional equation while the two-equation models employ two additional equations. All models use the eddy viscosity hypothesis; that is, the Reynolds stress, heat flux, and kinetic energy flux terms are assumed to be related to the mean-flow velocity, temperature, and kinetic energy gradients through an eddy transport coefficient. The same hypothesis is used for the second field variable in the two-equation models. Additional restrictions on the equations include the perfect gas assumption, constant specific heats, the Sutherland viscosity law, and zero bulk viscosity. The resulting equations, in divergence or conservation law form, can be written as follows:

$$\frac{\partial U}{\partial t} + \frac{\partial F}{\partial x} + \frac{1}{(R-y)^n}\frac{\partial [(R-y)^n G]}{\partial y} = H \qquad (1)$$

where

$$U = \begin{bmatrix} \rho \\ \rho u \\ \rho v \\ \rho e \\ \rho k \\ \rho s \end{bmatrix} \quad F = \begin{bmatrix} \rho u \\ \rho u^2 + \sigma_{xx} \\ \rho uv - \tau_{xy} \\ u(\rho e + \sigma_{xx}) - v\tau_{xy} + q_{Tx} \\ \rho uk + q_{kx} \\ \rho us + q_{sx} \end{bmatrix}$$

$$G = \begin{bmatrix} \rho v \\ \rho uv - \tau_{xy} \\ \rho v^2 + \sigma_{yy} \\ v(\rho e + \sigma_{yy}) - u\tau_{xy} + q_{Ty} \\ \rho vk + q_{ky} \\ \rho vs + q_{sy} \end{bmatrix} \quad H = \begin{bmatrix} 0 \\ 0 \\ -n\sigma_{\theta\theta}/(R-y) \\ 0 \\ H_k \\ H_s \end{bmatrix} \qquad (2)$$

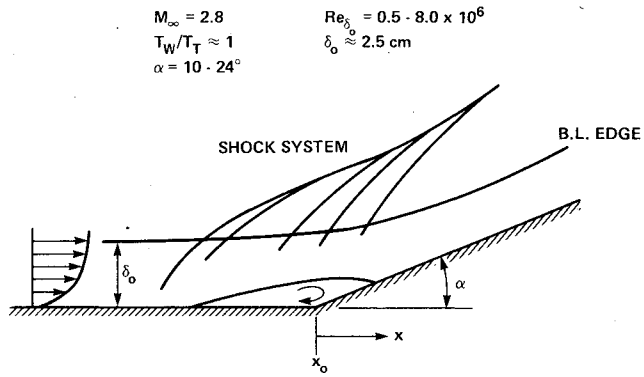

Fig. 3 Sketch of supersonic compression corner shock-wave boundary-layer interaction experiment.

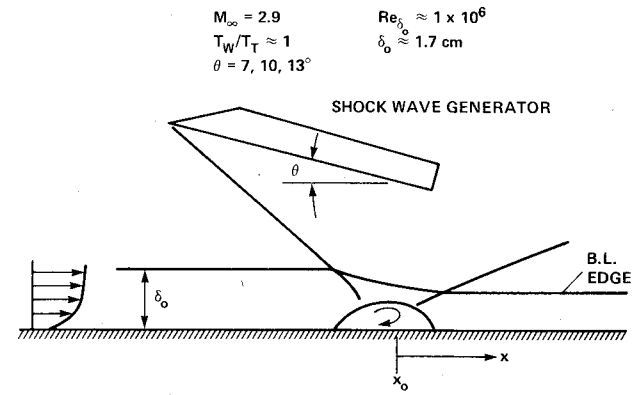

Fig. 4 Sketch of supersonic oblique shock-wave boundary-layer interaction experiment.

In the column vectors [F, G, and H] q_{Tx} and q_{Ty} are the total (laminar plus turbulent) heat flux vectors; σ_{xx}, σ_{yy} and $\sigma_{\theta\theta}$ are the total normal stresses; τ_{xy} is the total shear stress; and q_{kx}, q_{ky}, q_{sx} and q_{sy} are the flux vectors associated with the turbulence field variables.

Typical stress terms and flux vectors are

$$\sigma_{xx} = p + \frac{2}{3}\rho k - \tau_{xx}, \qquad \tau_{xy} = \mu_T\left(\frac{\partial u}{\partial y} + \frac{\partial v}{\partial x}\right)$$

$$\tau_{xx} = \frac{2}{3}\mu_T\left[2\frac{\partial u}{\partial x} - \left(\frac{\partial v}{\partial y} - \frac{nv}{R-y}\right)\right]$$

$$q_{Tx} = -K_T\frac{\partial T}{\partial x}, \qquad q_{kx} = -\mu_k\frac{\partial k}{\partial x}, \qquad q_{sx} = -\mu_s\frac{\partial s}{\partial x} \qquad (3)$$

where p is the hydrostatic pressure, $\frac{2}{3}\rho k$ is the pressure due to the kinetic energy of turbulence, K_T is the total thermal conductivity coefficient (including the eddy diffusivity effect), μ_T is the total viscosity; and μ_k and μ_s are the eddy diffusivities associated with the turbulence field variables. The perfect gas equation of state is used to relate hydrostatic pressure and temperature. The temperature is also related to the total energy per unit volume e by $e = c_v T + (u^2 + v^2)/2$. The functional form for the eddy diffusivities and the source functions H_k and H_s for the turbulence field variables are dependent on the turbulence model and will be discussed in the following section.

Equations (1) and (2) are written either for axially symmetric flow ($n = 1$) with its radial dimension y measured from the wall of the cylindrical control volume, of radius R, in a positive direction toward the centerline, or for plane flow ($n = 0$). For the corner flow problem, however, the equations

are complicated by a coordinate transformation introduced to allow one of the coordinate surfaces to conform to the corner wall boundary. These equations have been reported elsewhere[12] for the zero-equation turbulence models. The generalization that includes the one- and two-equation model equations is fairly straightforward and will not be given here.

Turbulence Models

The turbulence models used in this study are the zero-, one-, and two-equation eddy viscosity models. Many variations of each of these three types of eddy viscosity models exist[11,13-15] some of which have been investigated by the present authors, and many of which have yet to be investigated. In this paper a single representative of each of the zero- and one-equation model types and two representatives of the two-equation model types are summarized. This summary is purposely brief in the interest of emphasizing results. In Ref. 16 details of the models are presented along with additional results.

For all of the models the applicable diffusivities are expressible in terms of molecular and turbulent eddy viscosities as follows:

$$\mu_T=\mu+\mu_t, \qquad K_T=c_p\left[\left(\frac{\mu}{Pr}\right)+\left(\frac{\mu_t}{Pr_t}\right)\right]$$

$$\mu_k=\mu+\lambda_k\mu_t, \qquad \mu_s=\mu+\lambda_s\mu_t \tag{4}$$

where μ is the molecular viscosity, μ_t is the turbulent eddy viscosity, c_p is the constant pressure specific heat, Pr and Pr_t are the molecular and turbulent Prandtl numbers, respectively, and λ_k and λ_s are the coefficients associated with the turbulence field variables k and s, respectively. In the present investigation Pr and Pr_t are taken as 0.72 and 0.9, respectively. The expressions used for μ_t in the different turbulence models are outlined in the following paragraphs.

The zero-equation model investigated here is an equilibrium model. In this case the mean flow equations to be solved do not include the turbulence variables k and s, and the only modeling done is for the eddy diffusivities, which are modeled algebraically. The resulting expression for μ_t is one that agrees with the Prandtl-van Driest mixing length theory near the surface and with the Clauser formulation, supplemented by the Klebanoff intermittency factor away from the wall [see Eq. (6) of Ref. 16].

The one-equation or kinetic energy model uses, in addition to the mean flow equations, a partial differential equation for the kinetic energy of the turbulence k. The model used in the present study originated with Prandtl and Kolmogorov and was developed for incompressible flat plate boundary-layer flows by Glushko.[17] It was studied by Beckwith and Bushnell[18] in more complicated boundary-layer flows and was generalized by Rubesin[19] to compressible flows using mass-averaged variables.[20] The source function H_k for this model is given by Eqs. (9) and (10) of Ref. 16. The eddy viscosity for this model is a function of the Reynolds number of the turbulence, $R_t\equiv\rho\sqrt{k}\,L/\mu$. The functional form for μ_t in this case and the algebraic length scale of the turbulence L are given by Eqs. (11) and (12) of Ref. 16.

As discussed earlier, two two-equation models of turbulence are included in this investigation. These are the model of Jones and Launder[21] and the recently developed model of Wilcox and Rubesin.[11] Both models use two partial differential equations to simulate turbulence. The first equation in each case is the turbulent kinetic energy equation, as in the one-equation model. The second equation is for the turbulence variable s, which differs for each case, and is used in conjunction with k to define a turbulence length scale. In the Jones-Launder model, s is the turbulence energy dissipation rate and is given the symbol ϵ; in the Wilcox-Rubesin model, s is known as the square of the turbulent dissipation rate, $\omega(s\equiv\omega^2)$.

The Jones-Launder model was selected for this study because considerable experience has been gained in its application to simpler flows as well as the authors' recent adaptation of it to two of the SBLI flows.[10] The Wilcox-Rubesin model was selected because, as mentioned in the Introduction, it had been specifically developed to apply to boundary-layer flows influenced by severe adverse pressure gradients as well as to equilibrium flows.[11] Its accuracy had also been verified in recent studies at Ames Research Center using boundary-layer programs.[22]

The source functions—H_k and H_ϵ for the Jones-Launder model and H_k and H_{ω^2} for the Wilcox-Rubesin model—are given by Eqs. (14) and (18) of Ref. 16. For both models the eddy viscosity is a function of the turbulence Reynolds number, the length scale of which is determined from the turbulence field variables. $L=k^{3/2}/\epsilon$ and $L=\sqrt{k}/\omega$ for the Jones-Launder and Wilcox-Rubesin models, respectively. Explicit expressions for μ_t for these two-equation models are given by Eqs. (15) and (20) of Ref. 16. The Wilcox-Rubesin model differs from each of the other models in that the constitutive relation between the Reynolds stress tensor and the mean flow properties has an additional term which represents anisotropic normal Reynolds stress phenomena. The stress tensors for this model are given by Eq. (21) of Ref. 16.

Numerical Method and Boundary Conditions

The numerical procedure used here is the basic explicit second-order, predictor-corrector, finite-difference, time-splitting method of Mac Cormack[23] modified by the efficient explicit-implicit-characteristic algorithm of Ref. 1. The modifications apply near the surface and result from replacing the basic explicit operator that accounts for effects of the y derivative of Eq. (1) with a combination of more efficient operators. A description of the new method, along with its adaptation to multiequation turbulence model equations, is contained in Ref. 24. Also contained in Ref. 24 is a description of the boundary conditions and special procedures used for the turbulence model variables and equations. Reference 16 contains additional detailed discussion of the boundary conditions for the ω^2 equation of the Wilcox-Rubesin model.

Application of the numerical procedure to each of the flows studied was conceptually similar. The computational domain is divided into a two-mesh system. An exponentially stretched fine mesh is used near the wall to resolve that part of the flow where viscous effects are important; the outer flow, which is predominantly inviscid, is described using a uniform coarse mesh. A uniform mesh is also used in the flow direction. The number of mesh points used and the minimum spacing near the wall varied with the problem and the turbulence model. Generally, the first mesh point adjacent to the wall is selected such that moving it any closer to the wall would not significantly alter the solutions. For the zero-equation model the first mesh point off the wall is taken within the viscous sublayer ($y^+_{\min.}\equiv y\sqrt{\tau_w\rho_w/\mu_w}\lesssim 4$); for the higher-order models, the minimum y^+ required was smaller by a factor of 10 or 20. Typical mesh sizes were 40 points in the streamwise direction and 35 points normal to the wall (with 23 to 30 points in the boundary layer). In each problem, transfer from the exponentially stretched fine mesh to coarse mesh occurs near the outer edge of the boundary layer.

The boundary and initial conditions for the axisymmetric transonic SBLI flow have been adequately described in Refs. 2 and 25 for the mean-flow variables and in Ref. 24 for the turbulence variables. The boundary and initial conditions for the compression corner SBLI flow are described in Ref. 4. For the oblique SBLI flow the conditions are similar to those for the compression corner except along the upper boundary where the jump conditions for the oblique shock wave were imposed, and the upstream boundary which required a normal pressure gradient through the boundary layer.[7] The

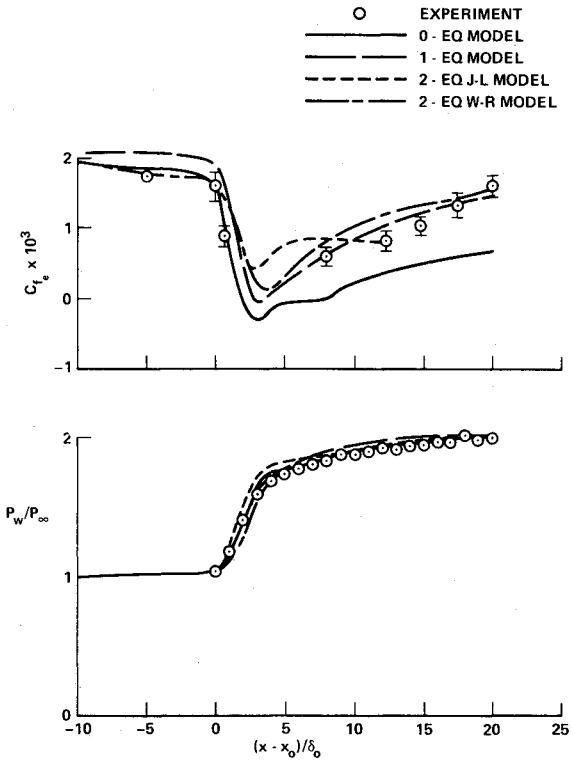

Fig. 5 Comparison of computations and surface measurements (skin friction and surface pressure) for the axisymmetric transonic SBLI experiment: $Re_{\delta_0} = 5.5 \times 10^5$, $M_\infty = 1.44$.

boundary and initial conditions for the turbulence variables for the compression corner and oblique SBLI flows were obtained in a manner similar to the methods described in Ref. 24.

For the two-dimensional transonic SBLI flow the boundary and initial conditions for the mean flow and the turbulence variables are described completely in Ref. 16. For each of the flows, variations of the initial level of the turbulence parameters were tried and found not to influence the converged solutions.

Results

Results for the axially symmetric transonic SBLI problem are presented in Figs. 5 and 6; those for the two-dimensional SBLI problem in Figs. 7 and 8; those for the supersonic compression corner SBLI in Figs. 9-11; and those for the supersonic oblique SBLI problem in Figs. 12-14. The measurements are described in Refs. 2-9. As mentioned in the Introduction, some results of the turbulence model SBLI flows investigated here have been given before: Refs. 2, 4, and 12 describe results of the zero-equation model for the axially symmetric and compression corner flows; Refs. 24 and 25 describe results for variants of the zero- and one-equation models for the axially symmetric problem; and Ref. 10 describes results for the Jones-Launder two-equation model and basic versions of the zero- and one-equation models for the axially symmetric and compression corner flow problems.

In the present paper, two additional flows are studied, the two-dimensional transonic and the supersonic oblique SBLI flows, with the zero-, one-, and Jones-Launder two-equation models as well as an investigation of all four flows with the new Wilcox-Rubesin two-equation model. The results of this study are discussed below in separate sections for each flow. Additional results for all four flows can be found in Ref. 16.

Transonic Axially Symmetric Shock-Wave Boundary-Layer Interaction

For the axially symmetric transonic flow problem, computations using the various turbulence models described in the text are compared with experimental measurements of surface pressure and skin friction. Also presented are comparisons of measured kinetic energy of turbulence profiles with calculations using the one-equation model and both two-equation turbulence models.

Surface Parameter Predictions

Comparisons of skin-friction and surface-pressure distributions for the axially symmetric transonic SBLI are shown in Fig. 5 for a Reynolds number Re_{δ_0}, just ahead of the shock, of 5.5×10^5. The experimental skin-friction results are from Ref. 2; the wall-pressure measurements, normalized by the freestream value about 37.5 cm ahead of x_0, are taken from some recent work of Mateer.[28] Considering first the results for the zero-equation model, one finds that the measured pressure distribution is very well predicted. Upstream of the calculated separation point, the measured and calculated skin-friction distributions also agree; however, downstream of this point, the calculations are in considerable disagreement with the measurements. (Mateer, in some very recent work,[29] has shown that, contrary to results stated in Refs. 2, 10, 24, and 25, the flow in this SBLI did not separate.)

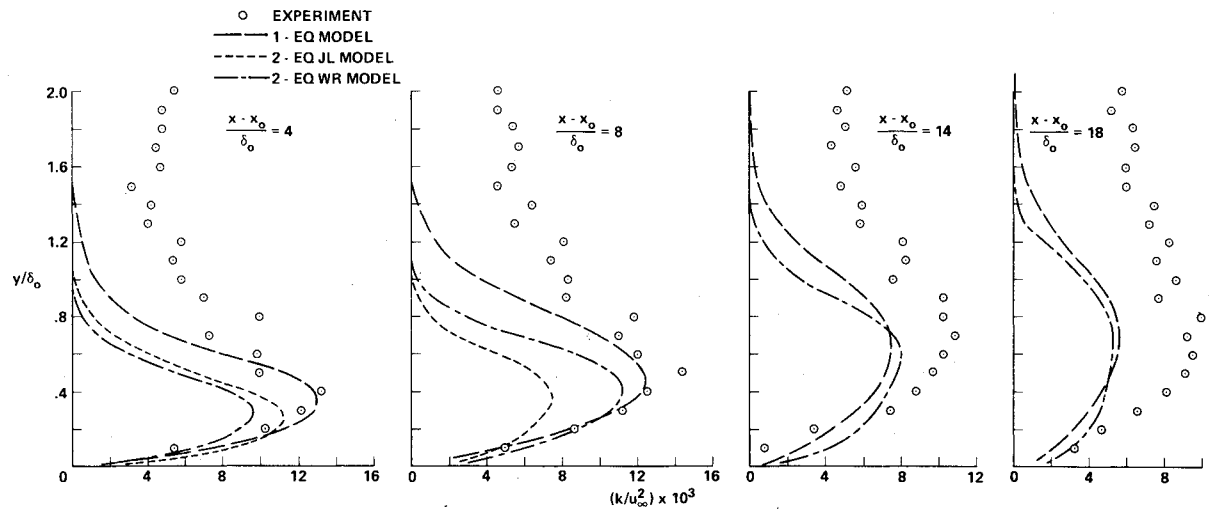

Fig. 6 Comparisons of computations and turbulent kinetic energy profile measurements for the axisymmetric transonic SBLI experiment: $Re_{\delta_0} = 5.5 \times 10^5$, $M_\infty = 1.44$.

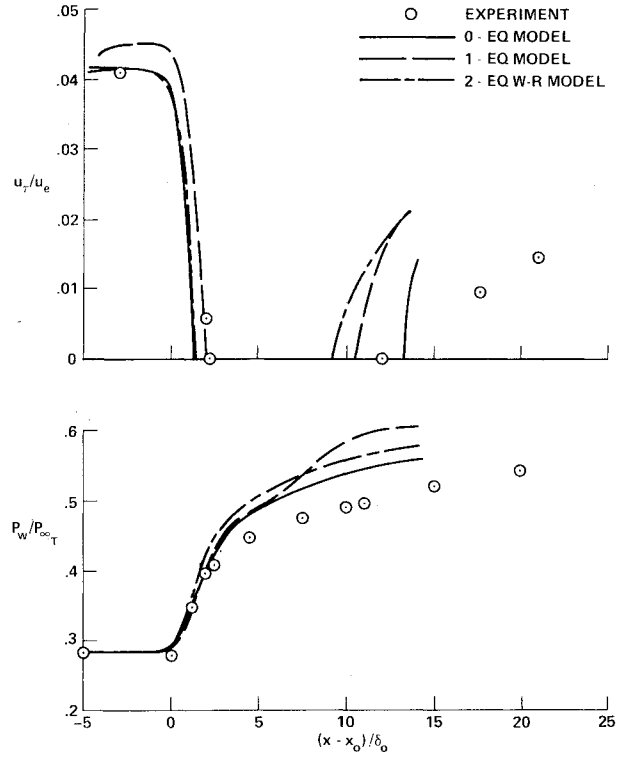

Fig. 7 Comparison of computations and surface measurements (shear velocity and surface pressure) for the two-dimensional transonic SBLI experiment: $Re_{\delta_0} = 5.3 \times 10^4$, $M_\infty = 1.47$.

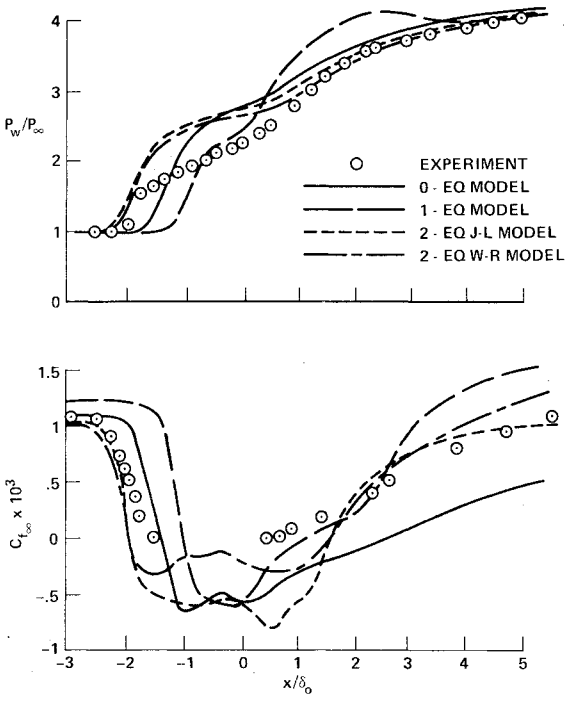

Fig. 9 Comparison of computations and surface measurements (surface pressure and skin friction) for the supersonic compression corner SBLI experiment: $\alpha = 24$ deg, $Re_{\delta_0} = 1.33 \times 10^6$, $M_\infty = 2.8$.

The one-equation model solution in Fig. 5 also agrees well with the measured pressure distribution. But, in addition, it predicts the measured rise in skin friction downstream of calculated reattachment significantly better than does the zero-equation model solution. This one-equation model, however, does not agree well with the skin-friction measurements near the upstream boundary and in the initial portion of the interaction region.

Results obtained with the Jones-Launder (J-L) two-equation model are also shown in Fig. 5. Solutions with this model seemed to be sensitive to the numerical grid spacing in the streamwise direction in and downstream of the interaction. Consequently, the grid spacing in the separation and reattachment zones was reduced by a factor of 8 relative to that used by the other models, and the range of $(x-x_0)/\delta_0$ was restricted from 0 to 12. The two-equation results shown are in substantial agreement with the measured pressure distribution. Also, the calculated flow did not separate and the skin-friction predictions are in agreement with the experiment at the upstream and downstream boundaries. However, qualitatively the calculated skin friction between the boundaries looks less like the experimental results than do the results of the previously discussed one-equation model. Replacing the equilibrium kinetic energy profile used at inflow boundary in this case by a more appropriate one taken from a one-equation model solution at $x = x_0$, as suggested in Ref. 10, did not significantly alter the results.

For this particular problem it has not yet been possible to obtain a steady solution using the Wilcox-Rubesin (W-R) two-equation turbulence model with the anisotropic normal Reynolds stress terms [Eq. (21) of Ref. 16] included. With these terms in the algorithm the results oscillated with time. Thus, for this particular configuration the W-R results are based on W-R two-equation model with the ansiotropic stress terms set to zero. In Fig. 5, this W-R two-equation model

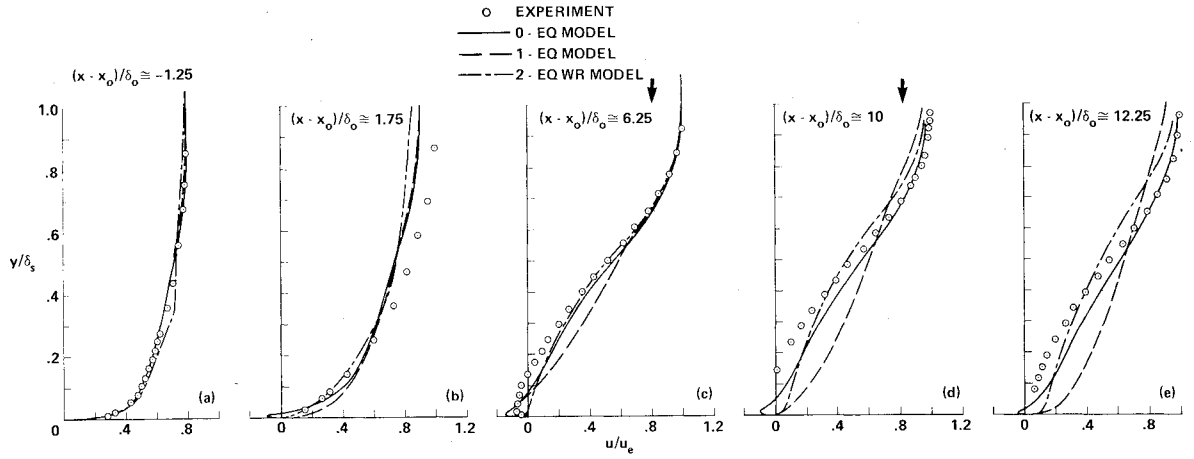

Fig. 8 Comparison of computations and velocity profile measurements for the two-dimensional transonic SBLI experiment: $Re_{\delta_0} = 5.3 \times 10^4$, $M_\infty = 1.47$.

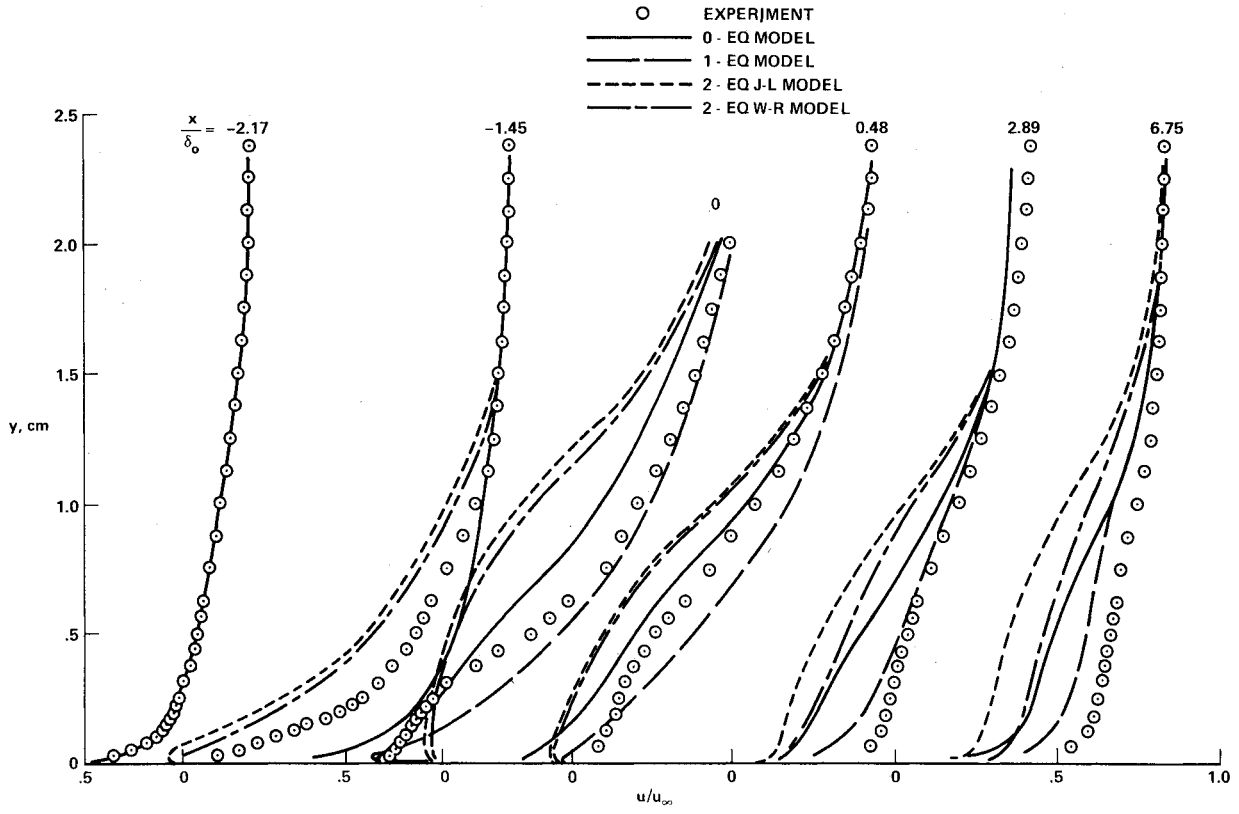

Fig. 10 Comparison of computations and velocity profile measurements for the supersonic compression corner SBLI experiment: $\alpha = 24$ deg, $Re_{\delta_0} = 1.33 \times 10^6$, $M_\infty = 2.8$.

solution also agrees very well with the measured pressure distribution. It also seems to give the best overall agreement with the measurements of skin friction. It agrees with the data upstream and downstream of the interaction region and does not predict flow separation.

Kinetic Energy Comparisons

Computed and measured profiles of the kinetic energy of turbulence are shown in Fig. 6. The measured kinetic energy was determined from a measurement of v' (see Fig. 12 of Ref. 2) and the assumption that $u'^2 : v'^2 : w'^2 = 4:2:3$. This assumption was observed recently to be reasonable for equilibrium flows at high subsonic Mach numbers.[26]

The shock wave has a very strong influence on the kinetic energy of the turbulence. Ahead of the shock, the peak value of k is very close to the wall,[10] at $y/\delta_0 \lesssim 0.01$, with a magnitude of about $0.007\, u_\infty^2$. As the pressure rises rapidly, owing to the shock, the turbulence energy increases and its peak moves away from the wall. Downstream of this rapid pressure rise, the peak turbulence decays with distance. Far from the shock, one would expect to recover a profile similar to that ahead of the shock.

It is apparent from Fig. 6 that the computed and measured profiles of the kinetic energy of turbulence are generally similar and that the trends with distance are in agreement. The J-L two-equation model seems to yield the most rapid decay of turbulence with x. The one-equation model yields the best agreement with the experiment for the peak and extent of turbulence with the W-R two-equation model a close second in this regard, especially downstream of the interaction. The experimental results do show a significant amount of freestream turbulence downstream of the shock. Though not shown on this figure, preliminary calculations have been made for this flow using the W-R two-equation model with the experimental level of freestream turbulence included downstream of the shock. These calculations show that it is possible to compute turbulence kinetic energy profiles that are in better agreement with the experimental results of Fig. 6 far from the surface without significantly increasing the value of skin friction relative to that shown on Fig. 5.

Transonic Two-Dimensional Shock-Wave Boundary-Layer Interaction

For the two-dimensional flow problem, computations using three of the four turbulence models described in the text are compared with experimental measurements of shear velocity, surface pressure, and velocity profiles. Converged solutions were not obtained when the J-L two-equation turbulence model was used for this flow problem and thus no solutions with this model are presented.

Surface Parameter Predictions

Comparisons of shear velocity (to be consistent with Seddon's data) and surface pressure distributions for the two-dimensional transonic SBLI are shown in Fig. 7 for a Reynolds number based on δ_0, just ahead of the shock, of 5.3×10^4. Although the numerical solutions with each model predict the location of the foot of the shock and the rate of initial pressure rise well, none of the calculations predicts the surface pressure in the separated and reattachment regions. An unsuccessful attempt was made to obtain improved agreement with the measured distribution by assuming that the shock wave was slightly oblique at the upper boundary rather than the normal shock reported by Seddon.[3] With a shock wave angle of 80 deg the surface pressure was reduced by about 5% but the foot of the shock moved $2\delta_0$ further downstream and the initial rate of pressure rise decreased by about 30%. Although Seddon's measurements gave some evidence that the flow was two-dimensional,[3] it is suspected that three-dimensional effects might account for the differences between the calculated and measured pressures. Sidewall boundary-layer buildup could result in an effective area reduction, which in the subsonic portion of the ex-

periment would lead to a pressure decrease. The calculated results presented here assume the flow is two-dimensional and the boundary conditions match as closely as possible those given by Seddon. The length of the control volume for the calculation is dictated by the farthest downstream location at which pressure profile data are given by Seddon.[3] This pressure profile is used with the time-dependent method of characteristics to obtain a downstream boundary condition for the subsonic flow which occurs in this case. This type of downstream condition, with a uniform exit pressure, is discussed in detail in Ref. 2. The outflow conditions in the boundary-layer region here are also treated as are those in Ref. 2.

As evident from the comparison of the surface shear velocity, the computations with all of the turbulence models predict flow separation. The zero-equation model and the W-R two-equation model results agree with the experiment ahead of the interaction where the one-equation result is high. The one-equation model is best at predicting the separation point and the extent of separation. None of the models predicts the location of reattachment or the level of wall shear downstream of reattachment. This latter disagreement is probably associated with the higher calculated pressures of Fig. 7.

Velocity Profile Comparisons

Figure 8 shows comparisons between measured and computed velocity profiles for the two-dimensional transonic SBLI experiment at various locations along the x axis. In these plots δ_s is the local boundary-layer thickness as determined by Seddon[3] and u_e is the velocity at the boundary-layer edge as determined by each calculation or by the experiment. Ahead of the foot of the shock (at $x-x_0 \simeq -1.25\delta_0$) all of the calculated velocity profiles are in good agreement with the data. At the inflow boundary of the calculations (taken as $x-x_0=-4.75\delta_0$) the velocity profiles are all identical, having been determined from a flat-plate calculation with the W-R two-equation model. The kink in the W-R model result at $y/\delta_s \simeq 0.35$ and $x-x_0 \approx -1.25\delta_0$ appears to be associated with some upstream influence of the pressure rise.

At $x-x_0 \simeq 1.75\delta_0$ the W-R model result looks most like the data near the wall. The zero-equation model result has already separated. The boundary-layer thickness for each of the models is larger than δ_s at this axial location as evidenced by the fact that calculated values of u/u_e are less than unity when $y=\delta_s$. At $x-x_0 \simeq 6.25\delta_0$ the calculations all show reversed profiles. The lower-order models have the largest flow reversal, but their zero velocity line is still too close to the surface and the curvature of their velocity profiles in this region does not match that of the experiment. Except for the lack of a significant region of flow reversal, the curvature of the velocity profile of the W-R model looks like the data. The overall shape of the velocity profile of the one-equation model looks least like the data.

At $x-x_0 \simeq 10\delta_0$, only the zero-equation model results still show flow reversal. The overall velocity profile curvature is best predicted by the zero-equation model and by the W-R two-equation model. Downstream of experimental reattachment ($x-x_0 \simeq 12.25\delta_0$) it is again apparent that the one-equation model gives the poorest prediction of the curvature of the velocity profile and the boundary-layer thickness.

Supersonic Compression Corner Shock-Wave Boundary-Layer Interaction

For the compression corner flow problem, computations using the various turbulence models discussed in the text are compared with experimental measurements of surface pressure, skin-friction, and velocity profiles. One experimental test geometry is discussed, a 24-deg compression corner ($Re_{\delta_0}=1.33\times10^6$), although a 20-deg compression corner ($Re_{\delta_0}=1.65\times10^6$) has also been studied. Results for the 20-deg corner are reported in Ref. 16. Comparisons are also made with experimental measurements of the extent of separation ahead of the corner for a wide range of Reynolds numbers.

Surface Parameter Predictions

Comparisons of the computed and experimental surface-pressure and skin-friction distributions for the supersonic compression corner are shown in Fig. 9. The computations employing the zero-equation model predict the qualitative features of the flowfield reasonably well, considering the simplicity of the turbulence model, but a closer examination of the comparisons points out the deficiencies of the computations. The overall pressure rise is predicted well, but the location of the initial rise in pressure is not. Also, the computations do not predict a pressure "plateau." Comparing the skin-friction results, the computations predict the locations of separation well, but they do not predict the reattachment locations and substantially underpredict the skin friction downstream of reattachment. The computations employing the one-equation model show worse agreement with the experimental pressure distribution for the 24-deg case. However, the predicted location of reattachment and the downstream skin-friction level is in better agreement with the data than the zero-equation model prediction. The computations employing both two-equation models give almost identical results to each other except for the magnitude of the skin-friction in the separated flow region. These computations show the best overall agreement with the experimental pressure distribution. The pressure "plateau" is predicted, although the level of the plateau is somewhat higher than was measured in the experiments. The predicted skin-friction results show that the forward extent of separation is slightly overpredicted. These comparisons show that the two-equation models are clearly superior for predicting the surface pressure distribution and that no single model predicts the correct skin-friction distribution although the one- and two-equation model results are slightly better than the zero-equation results. The W-R results shown here are for the isotropic Reynolds stress model. Stable solutions with the anisotropic terms included could not be obtained for this case. For the 20-deg case, solutions were obtained with and without this term (see results in Ref. 16). Based on those results the anisotropic terms have the largest effect on the calculated skin friction, lowering it by about 10% downstream of reattachment but have little effect on the other comparisons.

Velocity-Profile Predictions

Measured and computed velocity profiles throughout the flowfield are shown in Fig. 10. The computed results are only shown when they differ from the zero-equation model results. The zero-equation model predictions show general disagreement with experiment, and the one-equation model predictions show substantial improvement downstream of reattachment. This is consistent with the skin-friction results discussed previously. The computations employing both two-equation models give similar results. Both two-equation results predict much too large a retarded flow at the corner ($x/\delta_0=0.0$) and similar shaped profiles persist far downstream in general disagreement with the data. This indicates that both two-equation models have too large a memory effect downstream of a large separated region.

Prediction of Reynolds Number Effects

Because the previous detailed comparisons indicate that the separation location can be predicted reasonably well using any of the models tested, it is of interest to test these predictions against the Princeton experiments where separation locations and other data have been obtained for a wide range of Reynolds numbers. Solutions employing the zero-, one-, and two-equation turbulence models have been obtained for the range of experimental test conditions.

The computed extent of separation Δx_s ahead of the corner using the various turbulence models is compared with the experimental values in Fig. 11. For a corner angle of 20 deg, the results of the zero-equation model and of both two-equation models are in good agreement with the data over the entire Reynolds number range. The one-equation model results show the correct Reynolds number trend but underpredict the data. For a corner angle of 16 deg the computed results predict too large a decrease in separation distance with Reynolds number. However, a large portion of this disagreement could be caused by the coarse streamwise grid spacing which was $\sim 0.1\delta_0$ for the computed cases, which represent a much larger percentage of the separation distance for the 16-deg case than the 20-deg case.

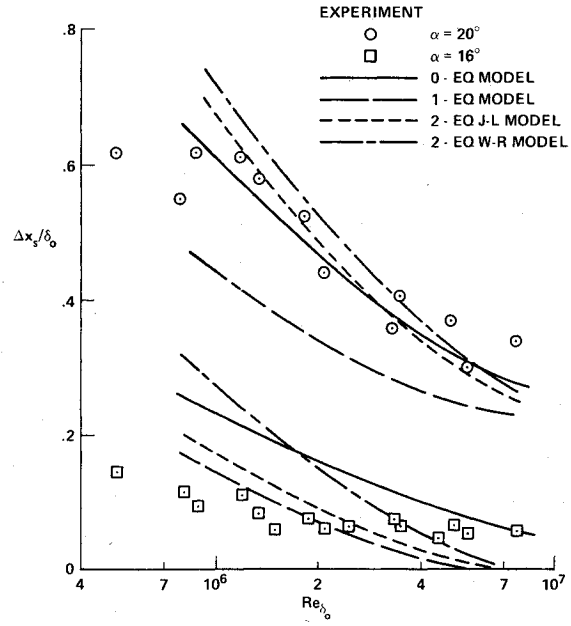

Fig. 11 Comparison of computations and measurements of the effect of Reynolds number on separation length for the supersonic compression corner SBLI experiment: $M_\infty = 2.8$.

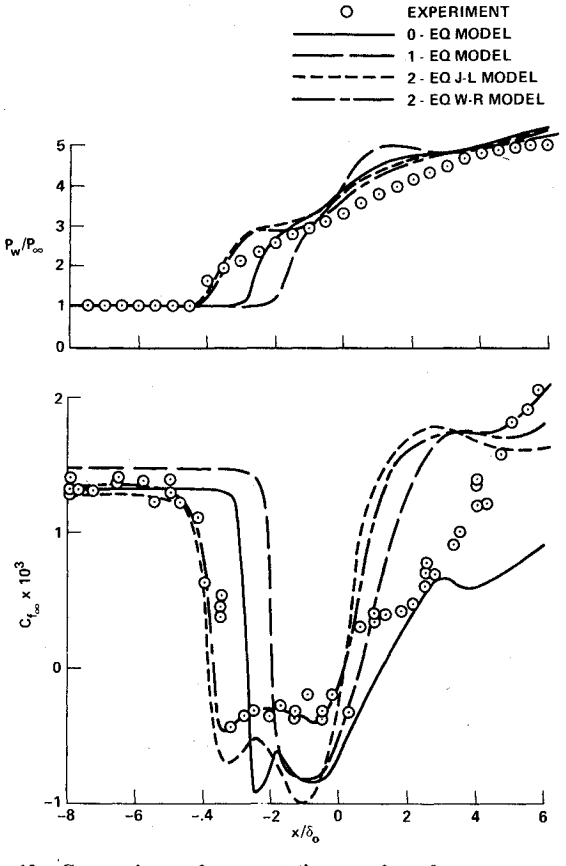

Fig. 12 Comparison of computations and surface measurements (surface pressure and skin friction) for the supersonic oblique SBLI experiment: $\theta = 13$ deg, $Re_{\delta_0} = 0.97 \times 10^6$, $M_\infty = 2.9$.

Supersonic Oblique Shock-Wave Boundary-Layer Interaction

For the oblique shock-wave boundary-layer interaction problem, computations using the various turbulence models discussed in the text are compared with experimental measurements of surface pressure and skin friction for a shock wave generator angle of 13 deg. Comparisons are also made with experimental mean velocity and turbulent kinetic energy profiles. Additional results for shock-wave generator angles of 7 deg and 10 deg are reported in Ref. 16.

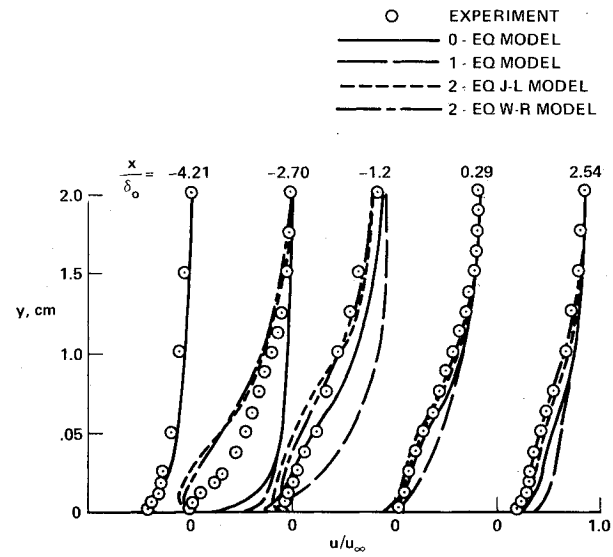

Fig. 13 Comparison of computations and velocity profile measurements for the supersonic oblique SBLI experiment: $\theta = 13$ deg, $Re_{\delta_0} = 0.97 \times 10^6$, $M_\infty = 2.9$.

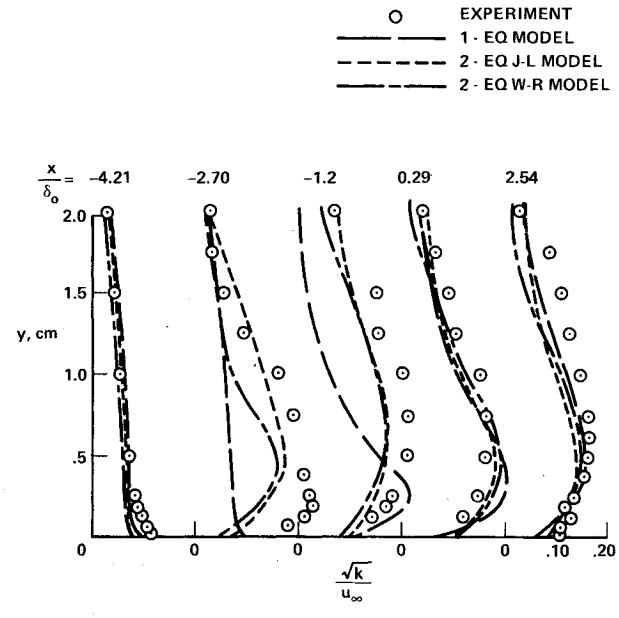

Fig. 14 Comparison of computations and turbulent kinetic energy profile measurements for the supersonic oblique SBLI experiment: $\theta = 13$ deg, $Re_{\delta_0} = 0.97 \times 10^6$, $M_\infty = 2.9$.

Surface Parameter Predictions

Comparisons of the computed and experimental surface-pressure and skin-friction distributions are shown in Fig. 12. The experimental flowfield contains a large separated region. For this flow the predicted pressure distribution comparisons are very similar to the previous comparisons for the compression corner experiment. The computations employing the one-equation model give the worst results and the computations employing both two-equation models give the best results, although the level of the pressure plateau is again overpredicted. The predicted skin-friction distributions yield large differences depending on the turbulence model employed and the shock wave strength computed. The comparisons of computed skin-friction results with the data are again similar to the comparisons for the compression corner. The downstream skin-friction levels and location of reattachment are better predicted by the one- and two-equation models. The location of separation is close to the zero- and two-equation results. However, the measured rise in skin friction following reattachment is not adequately predicted by any of the computations.

Velocity Profile Predictions

Measured and computed velocity profiles throughout the flowfield for $\theta = 13$ deg are shown in Fig. 13. In contrast to the compression corner results, both two-equation turbulence model results predict the data reasonably well, especially downstream of reattachment. The one-equation model computations give the worst results. These comparisons, which give opposite conclusions to similar comparisons for the compression corner, point out a fundamental difference between the two types of flow. The oblique shock-wave boundary-layer interaction flow has large downstream memory effects [note the similarity of the downstream velocity profile ($x/\delta_0 = 2.54$) to the one in the separated zone ($x/\delta_0 = -1.2$)] which are correctly predicted by the two-equation model computations. The compression corner shows very little downstream memory effect (possibly due to the thinning of the boundary layer or streamline curvature) where the computations still show large memory effects.

Turbulent Kinetic Energy Profile Predictions

Measured and computed turbulent kinetic energy profiles through the flowfield for $\theta = 13$ deg are shown in Fig. 14. (Since the experimental data only included measurements of streamwise and vertical velocity fluctuations, the lateral velocity fluctuations were assumed to be halfway between the streamwise and vertical velocity fluctuation to obtain the turbulent kinetic energy.) It is apparent that the computed results for both two-equation models and the measured profiles of the kinetic energy are generally similar. At reattachment ($x/\delta_0 = 0.29$) and downstream, the computations employing all three turbulence models agree quite well with the data. At separation ($x/\delta_0 = -2.7$) and in the separated zone ($x/\delta_0 = -1.2$), both two-equation model results are in better agreement with the data than the one-equation model results. However, at separation both two-equation model results fail to predict the high levels of kinetic energy measured (23%) near the wall.

Concluding Remarks

Numerical solutions of the compressible Navier-Stokes equations have been compared with and evaluated in terms of experimental measurements of four types of shock-wave turbulent boundary-layer interactions by using four different types of turbulence models. These models are mass-averaged versions of the zero-equation, one-equation, and the Jones-Launder two-equation eddy viscosity models of turbulence—all of which have been widely used for incompressible, unseparated, boundary-layer flows—and the newly developed Wilcox-Rubesin two-equation eddy viscosity model.

For the variety of flows studied, all of the turbulence models tested gave results that are in qualitative agreement with the experimental measurements. No single model gave the best quantitative agreement with each experiment but in general, overall improvement is obtained with higher-order turbulence models. Of the models tested, the W-R model results were most like the measurements for the range of conditions considered.

The two-equation models are the most attractive eddy viscosity models because of the way the turbulence length scale is calculated. With the zero- and one-equation models this length scale is usually defined as an algebraic function of the boundary-layer thickness, which is especially difficult and confusing to determine in separated or recirculating flows. The two-equation models, on the other hand, determined the length scale unambiguously from the solution of an additional turbulence field variable. The relative success of the W-R model at predicting the complex flows tested here may be due in part to it being developed for flows which included severe adverse pressure gradients and in part to it having simpler low Reynolds number terms which gave fewer numerical difficulties.[24,27]

Based on the results presented, the following specific conclusions can be made:

1) The surface pressure distributions are generally predicted more accurately by calculations using the two-equation models rather than the lower-order models.

2) Surface skin-friction comparisons are somewhat conflicting, with variants of the same type flows being better predicted by calculations with either the one- or two-equation models. Generally, zero-equation model results give the poorest predictions of this parameter.

3) No single model predicted the location of reattachment consistently, but again the consensus favors the higher-order models and, in particular, the W-R model.

4) For the flows that separate, the results of the zero-equation model predict location of the separation point best.

5) The velocity profiles downstream of the interaction are not predicted well by calculations using any of the models. This seems to be the main shortcoming of the higher-order models. One-equation model results are quickest to lead to a full profile downstream of reattachment.

6) Gross features of the kinetic energy of turbulence are in general fairly well predicted by calculations using any of the three higher-order models.

7) Predicted and measured Reynolds number effects are in good agreement for the compression corner for all four turbulence models. Even the variation of separation bubble size with Reynolds number for the transonic flows is consistent with these trends.

These conclusions are a bit general, as well they should be at the present stage of turbulence model development. The models used were derived for the most part phenomenologically with constants chosen so the models are applicable to equilibrium, often incompressible flow over flat-plate boundary layers. It is to the models' credit that they do so well in predicting the complex flows studied here.

The results were not obtained without a few numerical difficulties. These are discussed in the text or in the references. Some of the difficulties result from the fact that the models tested were not developed for complex flows. Some of these models have shortcomings which effect the numerics or the physics and some improvement in them is needed. Pressure gradient corrections have been developed for the zero-equation model.[4] These have been used by one of the authors and resulted in improved predictions of the measured skin-friction distributions. Similar effects might occur here.

The fact that the one-equation results always seem to yield high values of skin friction ahead of the interactions suggests that perhaps further tuning of this model is required. All

models could be improved by including effects of streamline curvature. The low Reynolds number terms in both two-equation models might also be improved for separated flows. The anisotropic terms in the W-R model, which have a tendency to increase skin friction and hence suppress separation, were troublesome and need further development for complex flows.

All of the differences between the predictions based on the calculations and the results of the measurements for these complex flows may not be strictly model dependent or numerical. The experimental flows themselves may be responsible. Three of the four flows tested could have possible complications resulting from three-dimensional effects which would prevent an accurate simulation by a two-dimensional analysis. Only the axially symmetric flow is truly two-dimensional, but it did not separate and thus does not provide a sufficiently complex flow for testing the models. A more appropriate test of the models could be provided by a well documented flow which has a large recirculation region and which is free of three-dimensional effects—such as an axisymmetric backward facing step. Such a flow would provide a more rigorous test of the present turbulence models and aid in their improvement or in the development of new models for recirculating flow.

References

[1] MacCormack, R.W., "An Efficient Numerical Method for Solving the Time-Dependent Compressible Navier-Stokes Equations at High Reynolds Number," *Computing in Applied Mechanics*, Applied Mechanical Div. Vol. 18, The American Society of Mechanical Engineers, 1976.

[2] Mateer, G.G., Brosh, A., and Viegas, J.R., "A Normal Shock-Wave Turbulent Boundary-Layer Interaction at Transonic Speeds," AIAA Paper 76-161, 1976.

[3] Seddon, J., "The Flow Produced by Interaction of a Turbulent Boundary Layer With a Normal Shock Wave of Strength Sufficient to Cause Separation," ARC R and M No. 3502, March 1960.

[4] Horstman, C.C., Settles, G.S., Vas, I.E., Bogdonoff, S.M., and Hung, C.M., "Reynolds Number Effects on Shock-Wave Turbulent Boundary-Layer Interactions," *AIAA Journal*, Vol. 15, Aug. 1977, pp. 1152-1158.

[5] Settles, G.S., "An Experimental Study of Compressible Turbulent Boundary Layer Separation at High Reynolds Number," Ph.D. Thesis, Dept. of Aerospace and Mechanical Sciences, Princeton Univ., Princeton, N.J., 1975.

[6] Settles, G.S., Vas, I.E., and Bogdonoff, S.M., "Details of a Shock-Separated Turbulent Boundary Layer at a Compression Corner," *AIAA Journal*, Vol. 14, Dec. 1976, pp. 1709-1715.

[7] Reda, D.C. and Murphy, J.D., "Shock Wave/Turbulent Boundary-Layer Interaction in Rectangular Channels," *AIAA Journal*, Vol. 11, Feb. 1973, pp. 139-140.

[8] Bachalo, W.D., Modarress, D., and Johnson, D.A., "Experiments on Transonic and Supersonic Turbulent Boundary Layer Separation," AIAA Paper 77-47, 1977.

[9] Murthy, V.S. and Rose, W.C., "Direct Measurements of Wall Shear Stress by Buried Wire Gages in a Shock Wave-Boundary Layer Interaction Region," AIAA Paper 77-691, 1977; also, *AIAA Journal*, Vol. 16, July 1978, pp. 667-672.

[10] Coakley, T.J., Viegas, J.R., and Horstman, C.C., "Evaluation of Turbulence Models for Three Primary Types of Shock Separated Boundary Layers," AIAA Paper 77-692, 1977.

[11] Wilcox, D.C. and Rubesin, M.W., "Progress in Turbulence Modeling for Complex Flow Fields, Including Effects of Compressibility," to be published as NASA TN.

[12] Hung, C.M. and MacCormack, R.W., "Numerical Simulation of Supersonic and Hypersonic Turbulent Compression Corner Flows Using Relaxation Models," AIAA Paper 76-410, July 1976.

[13] Launder, B.E. and Spalding, D.B., *Lectures in Mathematical Models of Turbulence*, Academic Press, London and New York, 1972.

[14] Reynolds, W.C., "Computation of Turbulent Flows," *Annual Review of Fluid Mechanics*, Vol. 8, 1976, pp. 183-208.

[15] Wilcox, D.C. and Traci, R.M., "A Complete Model of Turbulence," AIAA Paper 76-351, July 1976.

[16] Viegas, J.R. and Horstman, C.C., "Comparison of Multiequation Turbulence Models for Several Shock Separated Boundary-Layer Interaction Flows," AIAA Paper 78-1165, July 1978.

[17] Glushko, G.S., "Turbulent Boundary Layer on a Flat Plate in an Incompressible Fluid," *Bulletin of Academic Sciences USSR, Mechanical Series*, No. 4, 1965, pp. 13-23.

[18] Beckwith, I.W. and Bushnell, D.M., "Detailed Description and Results of a Method for Computing Mean and Fluctuating Quantities in Turbulent Boundary Layers," NASA TN D-4815, 1968.

[19] Rubesin, M.W., "A One-Equation Model of Turbulence for Use with the Compressible Navier-Stokes Equations," NASA TM X-73, 128, April 1976.

[20] Rubesin, M.W. and Rose, W.C., "The Turbulent Mean-Flow Reynolds-Stress and Heat Flux Equations in Mass-Averaged Dependent Variables," NASA TM X-62, 248, March 1973.

[21] Jones, W.P. and Launder, B.E., "The Prediction of Laminarization with a Two-Equation Model of Turbulence," *International Journal of Heat and Mass Transfer*, Vol. 15, Feb. 1972, pp. 301-314.

[22] Horstman, C.C., Kussoy, M.I., and Lanfranco, M.J., "An Evaluation of Several Compressible Turbulent Boundary-Layer Models: Effects of Pressure Gradient and Reynolds Number," AIAA Paper 78-1160, 1978.

[23] MacCormack, R.W., "Numerical Solution of the Interaction of a Shock Wave with a Laminar Boundary Layer," *Lecture Notes in Physics*, Vol. 8, Springer-Verlag, 1971, pp. 151-163.

[24] Coakley, T.J. and Viegas, J.R., "Turbulence Modeling of Shock Separated Boundary-Layer Flows," *Symposium on Turbulent Shear Flows*, University Park, Pa., April 18-20, 1977.

[25] Viegas, J.R. and Coakley, T.J., "Numerical Investigation of Turbulence Models for Shock Separated Boundary-Layer Flows," *AIAA Journal*, Vol. 16, April 1978, pp. 293-294.

[26] Acharya, M., "Effects of Compressibility on Boundary-Layer Turbulence," *AIAA Journal*, Vol. 15, March 1977, pp. 303-304.

[27] Rubesin, M.W., Crisalli, A.J., Horstman, C.C., Acharya, M., and Lanfranco, M.J., "A Critique of Some Recent Second Order Closure Models for Compressible Boundary Layers," AIAA Paper 77-128, 1977.

[28] Matter, G.G., private communication, June 1976.

[29] Mateer, G.G., private communication, March 1978.